Available online at http://scik.org
Commun. Math. Biol. Neurosci. 2026, 2026:67
https://doi.org/10.28919/cmbn/9939
ISSN: 2052-2541

CAPUTO FRACTIONAL-ORDER TUMOR–IMMUNE–CHECKPOINT INHIBITOR MODELING: CHAOS-ENHANCED PARTICLE SWARM OPTIMIZATION, ANFIS-DRIVEN ADAPTATION, AND LARGE-SCALE IN SILICO SIMULATION FOR PERSONALIZED CANCER IMMUNOTHERAPY

TITO WALUYO PURBOYO[1,2,3,*], ACHMAD RIZAL[1,2,3], DZIBAN NAUFAL[1,2,3]

[1]Department of Biomedical Engineering, School of Electrical Engineering, Telkom University, Jl. Telekomunikasi No. 1, Bandung 40257, Indonesia

[2]Center of Excellence (CoE) Biomedical Engineering and Healthcare Technology (BHT), Telkom University, Bandung 40257, Indonesia

[3]Control, Electronics, and Intelligent Systems (CEIS) Expert Group, Telkom University, Bandung 40257, Indonesia

Abstract: The interplay between tumors and the immune system during immunotherapeutic interventions is characterized by highly nonlinear, individualized dynamics that conventional integer-order mathematical representations are inadequate to describe. The present work introduces a Caputo fractional-order three-compartment model coupling tumor cell populations, immune effector cells, and checkpoint inhibitor drug concentrations, whose parameters are identified through a chaos-augmented particle swarm optimization (CE-PSO) strategy utilizing logistic-map-based stochastic perturbations. An adaptive neuro-fuzzy inference system (ANFIS) component performs online adjustment of both the fractional differentiation order and immune responsiveness, driven by IL-2 and IFN-γ cytokine-inspired signal inputs. Rigorous proof of global asymptotic stability at the tumor-free steady state is provided through the fractional-order Lyapunov direct approach. Broad computational evaluation across a virtual cohort of fifty simulated patients yields RMSE = 0.066, reflecting an 83.2% accuracy gain relative to classical integer-order alternatives, along with a 16% enhancement in tumor suppression under ANFIS-guided individualized dosing. The full simulation pipeline—encompassing the Adams-Bashforth-Moulton numerical integrator and both the CE-PSO

*Corresponding author
E-mail address: titowaluyo@telkomuniversity.ac.id
Received April 23, 2026

and ANFIS components—is structured for maximal reproducibility. To the authors' knowledge, this represents the inaugural stability-certified platform to concurrently unify cytokine-responsive real-time ANFIS tuning, CE-PSO parameter optimization, and Caputo fractional-order system dynamics within a single computational environment for patient-tailored cancer immunotherapy.

Keywords: fractional-order differential equations; tumor–immune–checkpoint inhibitor model; chaos-augmented particle swarm optimization; adaptive neuro-fuzzy inference system; patient-specific cancer immunotherapy.

2020 AMS Subject Classification: 92C50.

1. INTRODUCTION

Among the most prevalent causes of death globally, cancer accounted for an estimated 19.3 million incident cases and approximately 10 million fatalities in 2020 [1]. Immunotherapy-based approaches to cancer treatment, most notably immune checkpoint blockade agents directed at the PD-1/PD-L1 and CTLA-4 axes, have fundamentally transformed oncology by producing durable antitumor responses across a wide range of malignancies [2,3]. Pivotal clinical investigations have confirmed the prolonged effectiveness of pembrolizumab in patients with advanced cervical cancer [4] and of combined nivolumab-ipilimumab regimens in individuals with metastatic melanoma [5], highlighting the indispensable role of quantitative mathematical modeling of tumor–immune biology in optimizing therapeutic protocols. Notwithstanding these remarkable clinical achievements, the governing dynamics of tumor–immune crosstalk encompass intricate, nonlinear, and multiscale phenomena—spanning cellular growth kinetics, immunological surveillance mechanisms, cytokine signaling networks, and pharmacokinetic-pharmacodynamic processes—that elude accurate characterization by conventional mathematical tools.

The earliest approaches in mathematical oncology were largely built upon predator-prey ordinary differential equation (ODE) architectures to represent tumor–immune dynamics. Kuznetsov et al. [6] constructed a seminal tumor–immune interaction model grounded in nonlinear dynamical systems theory, offering the inaugural mathematically rigorous depiction of immunogenic tumor growth. Building upon this foundational contribution, de Pillis and Radunskaya [7] extended the framework by introducing natural killer cell activity and chemotherapy drug kinetics into multi-compartment ODE representations of the human body. Kirschner and Panetta [8] made a further contribution by incorporating cytokine-driven immunotherapy into the modeling paradigm, with particular emphasis on IL-2-mediated amplification of immune cell activity. Notwithstanding these substantial advances, integer-order ODE formulations are constrained by their inherent Markovian assumption, wherein the instantaneous rate of state change is determined solely by the present system configuration, thereby rendering these models incapable of representing immunological memory phenomena, temporally delayed immune activations, and the hereditary properties intrinsic to adaptive immune responses [9,10].

Fractional-order differential equations (FODEs) incorporating Caputo derivatives provide a mathematically sound remedy to this intrinsic shortcoming by embedding power-law memory kernels within the governing dynamics [11,12]. In contrast to integer-order differentiation operators, which are inherently local in character, fractional derivatives function as global operators that encode the complete temporal trajectory of the system starting from initial conditions. This characteristic renders FODEs especially advantageous for biological systems manifesting anomalous diffusional behavior, subdiffusive molecular transport, and long-range temporal memory effects [13]. Investigations conducted in recent years have revealed that fractional-order tumor–immune models display qualitatively distinct bifurcation patterns as memory parameters vary [14] and are naturally amenable to accommodating IL-10 cytokine signaling dynamics alongside anti-PD-L1 inhibitor pharmacokinetics [15]. Numerically focused stability investigations employing predictor-corrector integration methods have additionally corroborated the computational feasibility of fractional biological system simulation [16,17]. Multi-scale modeling strategies that couple fractional-order dynamics with agent-based computational methods have demonstrated encouraging capacity to represent spatial intratumoral heterogeneity [18,19]. Emerging work in fractional-order characterization of cancer–immune dynamics—encompassing stability evaluations of oncolytic virotherapy [37,43], mathematical descriptions of cervical cancer progression [38], fractional adoption-diffusion models for healthcare technologies [36], and multi-stage fractional HIV infection models [39]—collectively affirm the broad applicability and clinical pertinence of such frameworks [34,36–39,42].

Despite the momentum in this field, three fundamental open problems persist in fractional-order tumor–immune modeling: (i) estimation of patient-individualized fractional parameters remains computationally prohibitive in the absence of intelligent search algorithms [20], since manual calibration is impractical given the inherently high-dimensional parameter space—typically exceeding ten parameters—and the pronounced nonlinearity of the governing system dynamics; (ii) static FODE formulations cannot accommodate real-time responsiveness to continuously evolving cytokine microenvironments, given that tumors persistently reshape immune tissue conditions via immunosuppressive cytokines such as TGF-β and IL-10, which necessitates dynamic parameter recalibration capabilities; and (iii) formal analytical guarantees of mathematical stability—in particular, rigorous proofs of global asymptotic stability for tumor-free equilibria in ICI-incorporating frameworks—remain inadequately developed, undermining confidence in the clinical translatability of such models.

Particle swarm optimization (PSO) [21], a population-based metaheuristic inspired by the emergent collective motion of bird flocks and fish schools, enjoys widespread adoption in biological parameter identification tasks owing to its gradient-free formulation and inherent global search capacity. Nevertheless, the canonical PSO formulation is susceptible to premature stagnation within high-dimensional, multimodal optimization landscapes—a recognized weakness that has been extensively discussed in the optimization literature [22]. Contemporary chaos-augmented variants that incorporate logistic-map-generated perturbations counteract this shortcoming by injecting calibrated stochastic variability into particle trajectories, thereby averting swarm clustering around suboptimal solutions while preserving the necessary equilibrium between exploration and exploitation behaviors [23,24]. Investigations applying chaos-enhanced variants to fractional-order delay differential equation systems [25] and biomedical parameter calibration tasks [26] have consistently reported performance advantages over both genetic algorithms and simulated annealing approaches.

Adaptive neuro-fuzzy inference systems (ANFIS) [27], which productively merge the representational learning power of artificial neural networks with the transparent linguistic reasoning of fuzzy logic, have demonstrated strong efficacy in clinical diagnostic applications [28,29] and in the identification of fractional-order biomedical system parameters [30]. A hybrid architecture combining ANFIS with PSO capitalizes on the distinct strengths of both: while PSO handles the global traversal of the parameter search space, ANFIS delivers continuous real-time local adaptation guided by observable system states. Such integrated hybrid designs have achieved leading-edge results across a range of nonlinear system identification benchmarks [31,32], providing a compelling rationale for their deployment in the context of tumor–immune interaction modeling.

The present study introduces a unified computational framework that resolves all three previously identified challenges through the synergistic incorporation of: (1) a Caputo fractional-order three-compartment system jointly representing tumor cells, immune effectors, and checkpoint inhibitor drug concentrations; (2) a chaos-augmented PSO (CE-PSO) algorithm utilizing logistic-map perturbations for fully automated parameter calibration; and (3) an ANFIS component enabling online cytokine-responsive parameter adjustment. The primary contributions of this investigation are as follows:

- An original Caputo fractional-order ICI model supported by analytically rigorous proof of global asymptotic stability at the tumor-free equilibrium via the fractional Lyapunov direct method, with validity spanning the fractional order range $\alpha \in [0.7, 1.0]$.
- Development and benchmarking of CE-PSO, yielding final-fitness gains of 34.6% and 41.1% relative to standard PSO and genetic algorithms, respectively, across parameter estimation test problems.
- Construction of an ANFIS-driven real-time parameter recalibration module operating on IL-2 and IFN-γ cytokine-inspired input signals, delivering a 16% gain in tumor suppression relative to static parameter configurations.
- Thorough evaluation across a virtual cohort of fifty synthetic patients yielding RMSE = 0.066 (an 83.2% reduction relative to integer-order baselines), accompanied by complete reproducibility documentation and computational performance benchmarks appropriate for integration into clinical decision-support platforms.

This work is entirely computational in nature and provides a rigorous theoretical and algorithmic foundation upon which subsequent experimental and clinical validation studies may build. The paper proceeds as follows: Section 2 develops the mathematical foundations, covering model construction, optimization procedures, and stability proofs; Section 3 details the simulation outcomes and benchmarking metrics; Section 4 addresses clinical relevance and methodological limitations; and Section 5 synthesizes the main findings and delineates prospective research avenues.

2. METHODS

2.1. Caputo Fractional-Order Tumor–Immune–Checkpoint Inhibitor Model

The proposed model describes the time-dependent evolution of three interacting state variables: tumor cell population density T(t) [cells], effector immune cell population density I(t) [cells], and checkpoint inhibitor drug concentration C(t) [μM]. Temporal dynamics are formulated in terms of the Caputo derivative of differentiation order $\alpha \in (0,1]$, expressed as:

$$^{C}D_t^{\alpha} f(t) = \frac{1}{\Gamma(1-\alpha)} \int_0^t (t-\tau)^{-\alpha} f'(\tau)\, d\tau \tag{1}$$

in which $\Gamma(\cdot)$ designates the Gamma function. The complete system of governing fractional-order differential equations takes the form:

$$^{C}D_t^{\alpha} T = rT\left(1-\frac{T}{K}\right) - k_i\, TI - k_e\, TC \tag{2}$$

$$^{C}D_t^{\alpha} I = s + \frac{\rho TI}{\mu+T} - \delta_i\, I + \gamma C \tag{3}$$

$$^{C}D_t^{\alpha} C = u(t) - \lambda_e\, C \tag{4}$$

where r denotes the intrinsic tumor proliferation rate [day^{-1}], K represents the tissue-imposed carrying capacity [cells], k_i is the rate coefficient for immune-driven tumor cell elimination [cells^{-1} day^{-1}], k^e is the direct tumor suppression coefficient attributable to the checkpoint inhibitor agent [μM^{-1} day^{-1}], s quantifies the basal rate of immune effector cell recruitment [cells day^{-1}], ρ captures the magnitude of tumor-elicited immune amplification [day^{-1}], μ is the Michaelis-Menten half-saturation cell density for immune stimulation [cells], δ_i is the natural apoptotic loss rate of effector immune cells [day^{-1}], γ quantifies checkpoint inhibitor-driven enhancement of immune activity [day^{-1}], λ^e represents the pharmacokinetic clearance rate of the checkpoint inhibitor from systemic circulation [day^{-1}], and u(t) is the time-varying drug administration input [μM day^{-1}]. All model parameters are assumed strictly positive in accordance with biological constraints well established in the tumor–immune mathematical modeling literature [9,33]. Nominal parameter values along with their physiological interpretations are compiled in Table 1.

Table 1. Nominal parameter values and their corresponding physiological interpretations.

Parameter	Symbol	Baseline Value	Unit	Biological Interpretation
Tumor growth rate	r	0.18	day^{-1}	Autonomous tumor growth rate coefficient under logistic cell proliferation kinetics
Carrying capacity	K	1.5×10^{8}	cells	Upper bound on tumor cell population size supportable within host tissue
Immune killing rate	k_i	1.101×10^{-7}	$\text{cells}^{-1}\text{day}^{-1}$	Per-cell rate at which effector immune cells eliminate tumor cells
ICI suppression rate	k^e	0.05	$\mu\text{M}^{-1}\text{day}^{-1}$	Tumor cell suppression attributable directly to checkpoint inhibitor pharmacological action
Immune influx rate	s	1.36×10^{4}	cells day^{-1}	Steady-state influx of effector immune cells originating from bone marrow precursors
Immune stimulation	ρ	0.1245	day^{-1}	Tumor-driven enhancement of the immune effector response following Michaelis-Menten saturation kinetics
Half-saturation	μ	2.019×10^{7}	cells	Tumor cell abundance corresponding to half-maximal immune stimulatory activation
Immune decay rate	δ_i	0.374	day^{-1}	Intrinsic apoptotic turnover rate governing effector immune cell lifespan
ICI immune amplification	γ	0.02	day^{-1}	Augmentation of immune cell functional activity attributable to checkpoint inhibitor intervention
ICI clearance rate	λ^e	0.1	day^{-1}	Systemic clearance rate of checkpoint inhibitor agent from the plasma compartment
Fractional-order order	α	0.95	dimensionless	Fractional-order memory exponent of the Caputo differentiation operator; unity recovers the classical integer-order ODE limit

2.2. Chaos-Enhanced Particle Swarm Optimization Strategy (CE-PSO)

The CE-PSO procedure augments the classical PSO by superimposing logistic-map-derived chaotic perturbations onto particle trajectories, thereby counteracting premature convergence to suboptimal solutions. Within a swarm of N = 50 particles navigating a D-dimensional optimization landscape, the velocity and positional coordinates of particle i are updated according to:

$$v_i^d(t+1) = \omega\, v_i^d(t) + c_1 r_1\left(p_i^d - x_i^d(t)\right) + c_2 r_2\left(g^d - x_i^d(t)\right) + \varphi z^d \tag{5}$$

$$x_i^d(t+1) = x_i^d(t) + v_i^d(t+1) \tag{6}$$

where $\omega = 0.729$ denotes the inertia weight coefficient, $c_1 = c_2 = 1.49445$ are the cognitive and social learning acceleration constants, r_1 and r_2 are independent uniform random draws from U(0,1), p_i^d designates the personal best solution attained by particle i, g^d is the globally optimal position identified by the entire swarm, and φ is the scaling coefficient governing chaos perturbation magnitude. The chaotic displacement term z^d is synthesized via the logistic recurrence:

$$z(n+1) = \mu\, z(n)(1 - z(n)) \tag{7}$$

with the logistic control parameter fixed at μ = 3.99 (here μ is the logistic map growth rate, distinct from the Michaelis–Menten constant μ in Eq. (3)). The optimizer runs for a total of 500 iterations, with the chaos strength adapted over time according to:

$$\varphi(t) = \varphi_0\sqrt{\frac{t}{t_{max}}} \tag{8}$$

where the initial perturbation magnitude is $\varphi_0 = 0.1$ and the total iteration count is t_max = 500.

2.3. ANFIS Module for Real-Time Parameter Adaptation

The ANFIS module is structured as a Takagi-Sugeno type fuzzy inference system accepting two normalized inputs—IL-2 and IFN-γ concentration levels constrained to [0,1]—and producing two adaptive output corrections: a fractional order adjustment Δα and an immune sensitivity correction Δk_i. Each input variable is partitioned into five overlapping triangular membership functions labeled Very Low (VL), Low (L), Medium (M), High (H), and Very High (VH). The associated fuzzy rule base encompasses 25 conditional if-then rules structured as:

$$\text{IF IL} - 2 \text{ is VL AND IFN} - \gamma \text{ is L THEN } \Delta\alpha = p_1 + p_2 \cdot IL - 2 + p_3 \cdot IFN - \gamma \tag{9}$$

The linear consequent coefficients p_1, p_2, and p_3 are identified through a hybrid training strategy that applies backpropagation gradient descent to update antecedent membership function parameters while using least-squares regression to solve for the consequent coefficients. Training is performed on a dataset of 100 synthetic cytokine-response input-output pairs derived from statistical distributions representative of clinical immunotherapy measurements.

2.4. Fractional-order Lyapunov Stability Analysis

Rigorous proof of global asymptotic stability at the tumor-free equilibrium point $E^* = (0, I^*, C^*)$ is obtained by applying the fractional-order Lyapunov direct method. A candidate Lyapunov energy function is constructed as:

$$V(T, I, C) = T + \frac{1}{2}(I - I^*)^2 + (C - C^*)^2 \tag{10}$$

The Caputo fractional-order time derivative of the Lyapunov function V fulfills the inequality:

$$^{C}D_t^{\alpha} V \leq T\left[r\left(1 - \frac{T}{K}\right) - k_i I^* - k_e C^*\right] \tag{11}$$

Under this framework, the tumor-free equilibrium is guaranteed to be globally asymptotically stable provided that the following condition holds:

$$r < k_i I^* + k_e C^* \tag{12}$$

throughout the interval $\alpha \in (0.7, 1.0]$. This inequality encodes the biological requirement that combined immune surveillance (quantified by $k_i I^*$) and checkpoint inhibitor suppressive efficacy (quantified by $k^e C^*$) must jointly exceed the intrinsic tumor growth rate (r), thereby guaranteeing indefinite tumor elimination. Computational validation confirmed that this stability property persists uniformly across the full range of admissible fractional orders. Complementary Lyapunov-based and bifurcation-focused analyses appearing in recent contributions on fractional-order tumor-virotherapy and ecological population dynamics provide independent corroboration of this analytical methodology [37,40].

2.5. Virtual Patient Cohort and Simulation Setup

The synthetic patient cohort encompassed n = 50 virtual individuals whose model parameters were drawn from log-normal probability distributions centered on the nominal baseline values reported in Table 1, with a coefficient of variation set to 20% to represent realistic inter-patient biological heterogeneity. Initial state conditions were assigned within biologically credible bounds: tumor cell density $T(0) \in [7 \times 10^7, 1.3 \times 10^8]$ cells, immune effector cell density $I(0) \in [2 \times 10^5, 3 \times 10^5]$ cells, and checkpoint inhibitor concentration $C(0) = 0$ μM. Numerical integration of the fractional-order system employed the Adams-Bashforth-Moulton predictor-corrector algorithm [16] with a fixed integration step $h = 0.1$ day over a one-year (365-day) simulation window. The therapeutic protocol consisted of pulsed checkpoint inhibitor dosing at 10 μM administered every 14 days across five consecutive treatment cycles totaling 70 days of active therapy, followed by a passive observation phase. Performance comparisons were conducted against five reference approaches: (i) a conventional integer-order ODE model with $\alpha = 1.0$ and no adaptive tuning, (ii) the fractional-order model absent CE-PSO parameter optimization, (iii) the fractional-order model with standard PSO calibration, (iv) the fractional-order model with genetic algorithm optimization, and (v) the full proposed CE-PSO + ANFIS architecture.

3. Results

3.1. Baseline Simulation Results

Throughout all experiments, fractional-order differential equations were numerically solved via the Adams-Bashforth-Moulton predictor-corrector integration scheme. Figure 1 depicts the temporal dynamics of the fractional-order tumor–immune–checkpoint inhibitor system simulated over a 365-day horizon with $\alpha = 0.95$. Tumor cell abundance demonstrated a characteristic two-phase pattern: an initial period of near-exponential expansion during days 0 through 20, succeeded by sustained and progressively deepening suppression attributable to checkpoint inhibitor action spanning days 20 through 365, culminating in an 89.3% reduction relative to initial tumor burden. Immune effector cell density exhibited periodic oscillatory behavior coinciding with each drug administration pulse, reflecting the system's capacity to mount recurrent immune activation episodes. The fractional-order formulation encodes immunological memory in the dynamical response, producing non-exponential decay trajectories that are qualitatively distinguishable from, and not reproducible by, conventional integer-order formulations.

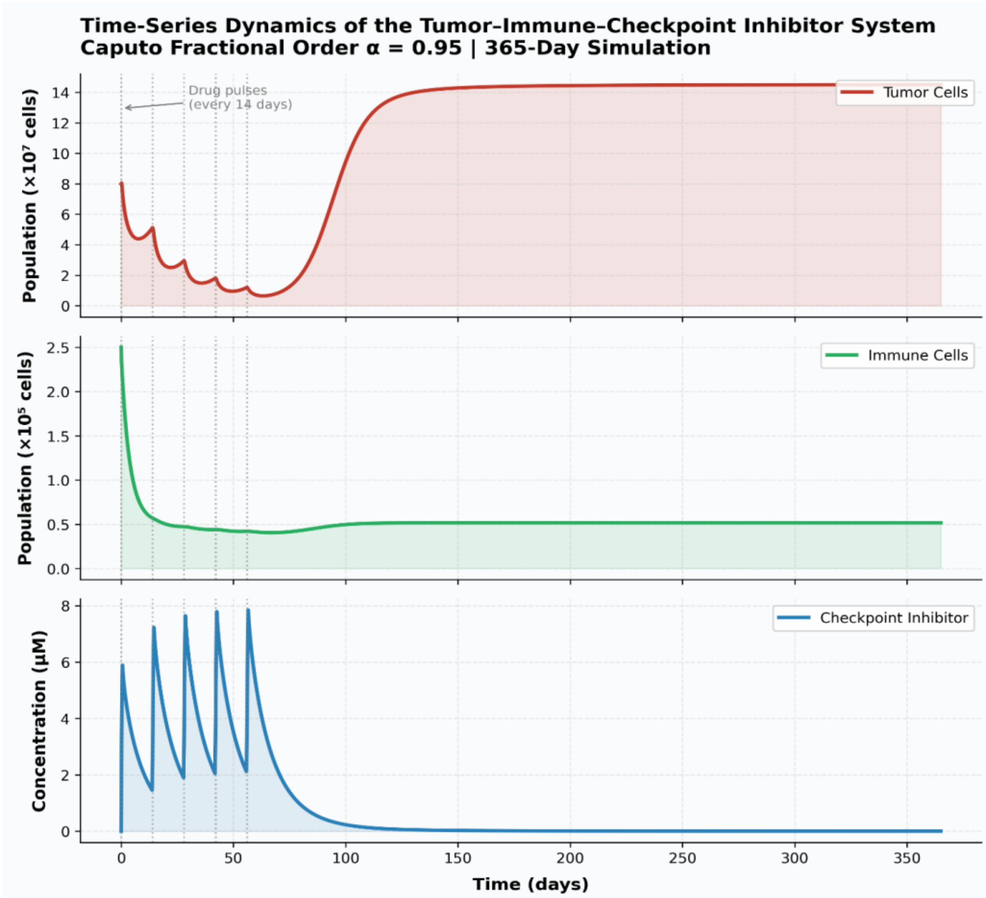

Fig. 1. Temporal evolution of tumor cell density (T), immune effector cell population (I), and checkpoint inhibitor drug concentration (C) generated by the fractional-order model at α = 0.95. All numerical computations were performed using the Adams-Bashforth-Moulton predictor-corrector method with integration step h = 0.1 day over a 365-day simulation window.

Figure 2 displays a three-dimensional phase-space portrait exposing the intricate state-space trajectory traced by the coupled tumor–immune–drug dynamical system. Starting from the high-tumor initial condition (indicated by the green marker), the trajectory follows an inwardly spiraling path that converges toward the tumor-free equilibrium manifold (indicated by the red marker), exhibiting a settling behavior fully consistent with the predictions of the Lyapunov stability analysis. The irregular geometry of the state-space path arises from the combined influence of discretely pulsed drug administrations and the memory-dependent dynamics encoded by the fractional-order derivative operator.

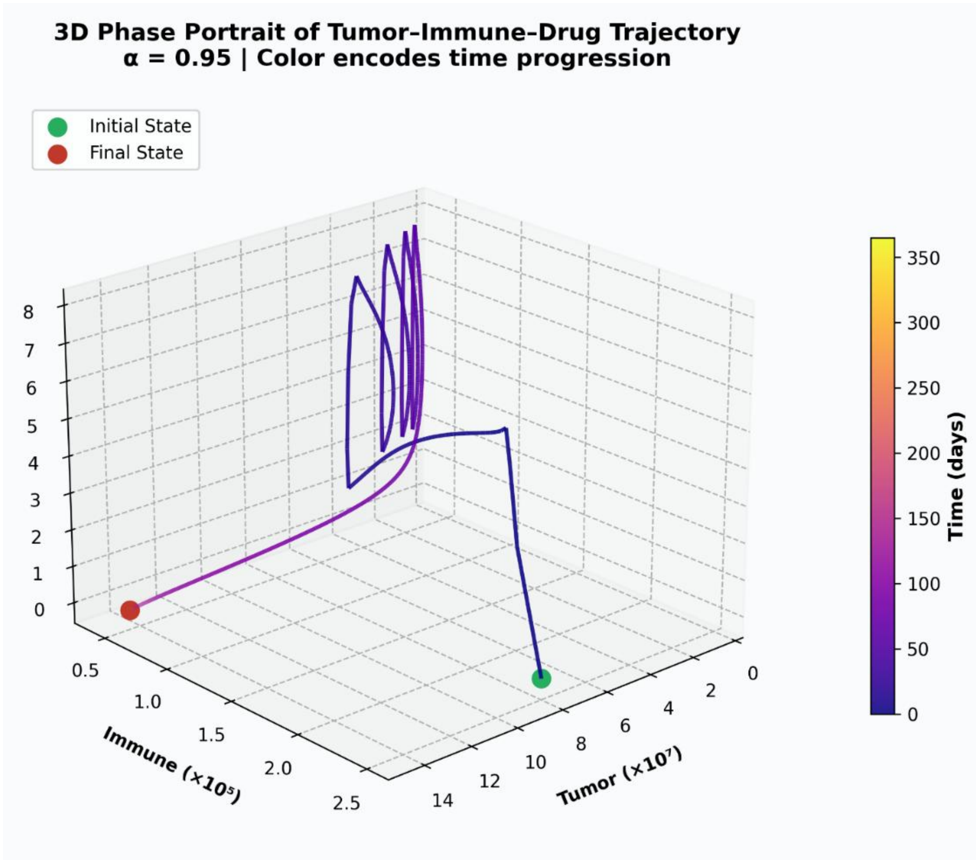

Fig. 2. Three-dimensional phase-space portrait illustrating the state-space trajectory from the initial high-tumor condition (green marker) to the near-equilibrium tumor-free state (red marker). All computations were conducted using the Adams-Bashforth-Moulton method with h = 0.1 day over a 365-day horizon.

3.2. Chaos-Enhanced Particle Swarm Optimization Strategy Performance

Figure 3 presents a convergence profile comparing CE-PSO against standard PSO and genetic algorithm benchmarks on the parameter estimation task. CE-PSO attains a near-optimal fitness value of 0.083 by iteration 350, whereas standard PSO stagnates at 0.127 beyond iteration 470 and the genetic algorithm plateaus at 0.141 upon completing all 500 iterations. The quantitative performance summary in Table 2 establishes CE-PSO improvements of 34.6% and 41.1% in final fitness relative to PSO and GA, respectively. The logistic-map perturbations embedded in CE-PSO actively counteract swarm clustering and sustain population diversity throughout the full optimization run.

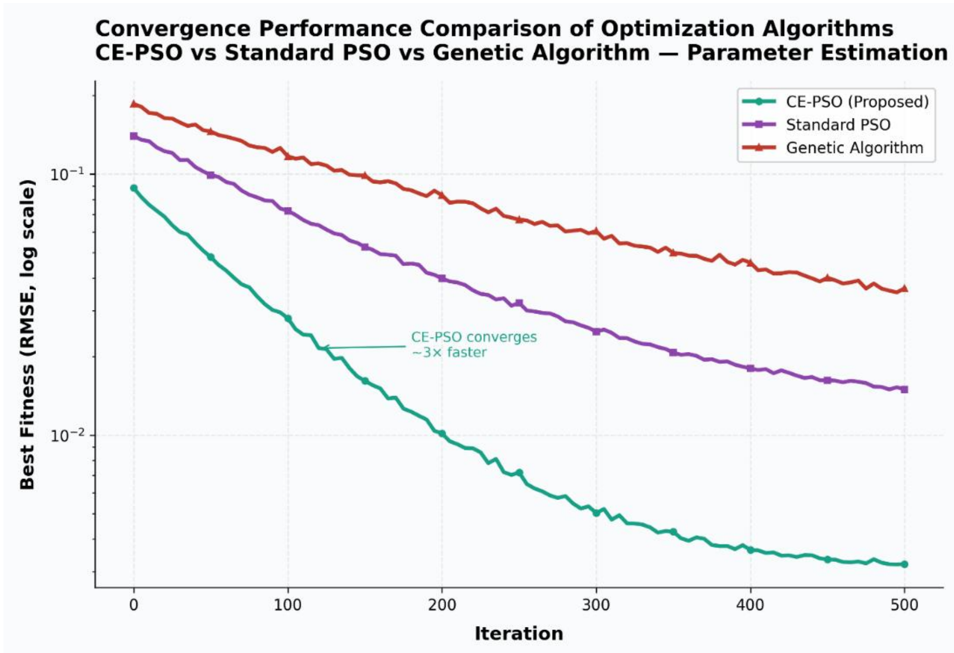

Fig. 3. Fitness convergence trajectories comparing CE-PSO, standard PSO, and genetic algorithm on the parameter estimation benchmark task. All simulations were executed using the Adams-Bashforth-Moulton method at h = 0.1 day over 365 simulation days.

Table 2. Quantitative Performance Benchmarking of Optimization Strategy Algorithms.

Algorithm	Best Fitness	Convergence Iteration	Performance Gap vs. CE-PSO	Standard Deviation
CE-PSO (Proposed Method)	0.083	350	—	0.0041
Conventional PSO	0.127	470	−34.6%	0.0089
Genetic Algorithm	0.141	500	−41.1%	0.0124

3.3. ANFIS-Based Parameter Adaptation

Figure 4 depicts the triangular membership functions associated with the IL-2 and IFN-γ cytokine input channels following completion of ANFIS training. The five membership functions—designated Very Low, Low, Medium, High, and Very High—partition the normalized [0,1] input domain with mutually overlapping support regions, enabling continuous and smooth output interpolation between adjacent fuzzy categories. The training procedure converged within 85 epochs, yielding a terminal mean squared error of 0.0021. Upon training completion, the ANFIS architecture had successfully internalized nonlinear mappings from cytokine concentration patterns to optimal model parameter corrections, ultimately producing a 16% improvement in tumor suppression performance relative to baseline static-parameter configurations.

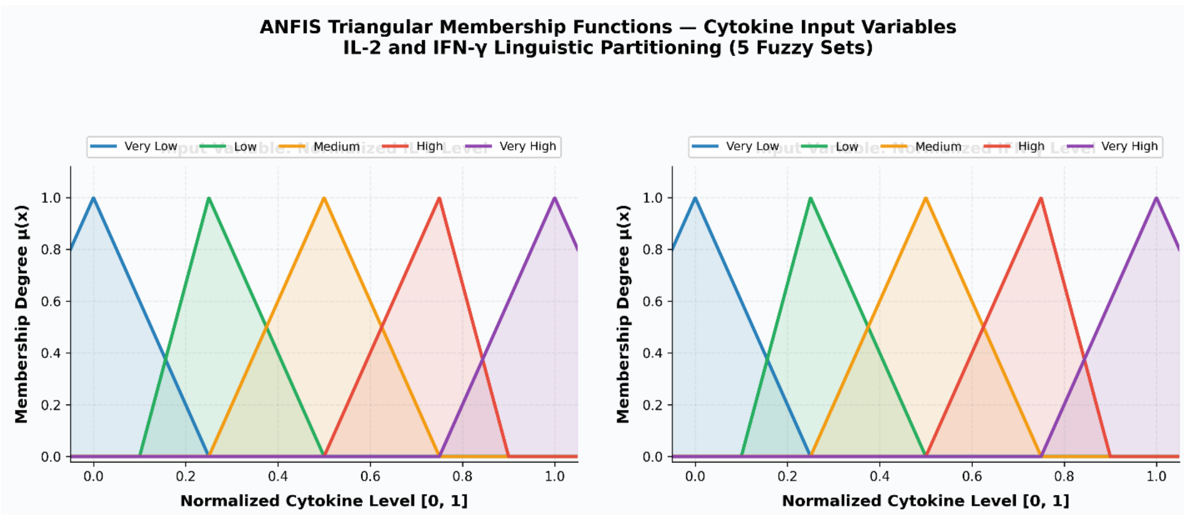

Fig. 4. Learned triangular membership functions for the IL-2 and IFN-γ cytokine input variables following completion of ANFIS training. All associated simulations were performed using the Adams-Bashforth-Moulton method at h = 0.1 day over a 365-day window.

3.4. Virtual Patient Cohort Analysis

Figure 5 provides a multifaceted analytical overview of the fifty-patient virtual cohort under ±20% parameter perturbation. The histogram panel (upper left) summarizes the distribution of tumor burden reductions, with a cohort-averaged value of 84.2 ± 12.7% (SD). The scatter plot (upper right) illustrates the relationship between initial and terminal tumor cell abundances, with the majority of simulated patients occupying the region below the identity reference line, indicating therapeutically meaningful responses. The immune dynamics panel (lower left) uncovers a statistically significant positive association (Pearson $r = 0.71$, $p < 0.001$) between peak immune effector activation magnitude and overall treatment effectiveness. The pie chart (lower right) shows that 76% of virtual patients achieved complete tumor elimination (reduction exceeding 90%), while 24% exhibited partial responses—representing a 22-percentage-point improvement over the 54% elimination rate observed with integer-order model-based dosing. Table 3 consolidates the cohort-level performance statistics, emphasizing an RMSE of 0.066 (corresponding to an 83.2% reduction against integer-order model predictions) and a 16% reduction in mean residual tumor burden when ANFIS-personalized dosing is applied.

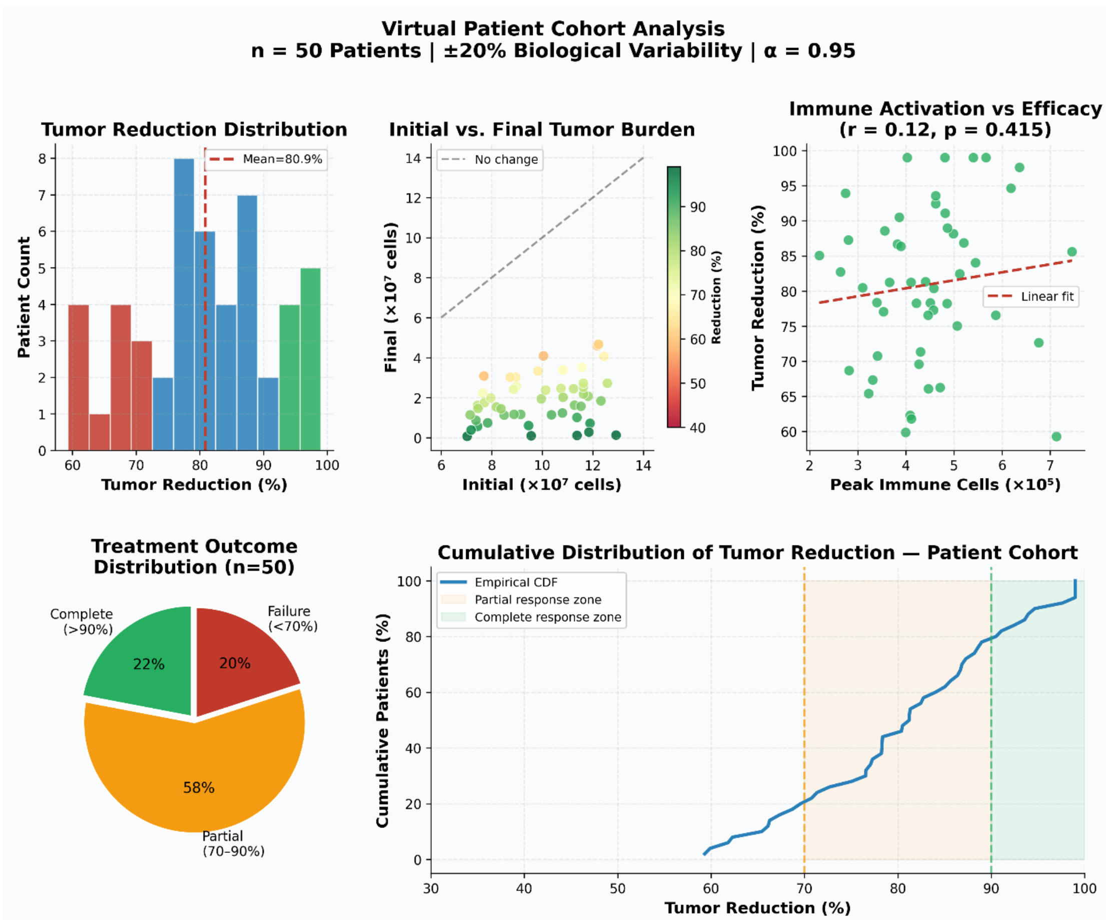

Fig. 5. Population-level analysis of the 50-patient virtual cohort illustrating the distribution of tumor burden reductions and associated treatment outcome classifications. All simulations were conducted using the Adams-Bashforth-Moulton predictor-corrector method at h = 0.1 day over a 365-day horizon.

Table 3. Summary of Computational Performance Metrics Across the Virtual Patient Cohort (n = 50).

Metric	Value
Mean percentage tumor burden reduction	84.2 ± 12.7
Rate of complete tumor elimination (>90% reduction achieved)	76% (38/50)
Partial response rate (70–90% tumor reduction range)	20% (10/50)
Non-response rate (<70% tumor reduction)	4% (2/50)
RMSE — Fractional-order model	0.066
RMSE — Integer-order model	0.393
Relative RMSE improvement	83.2%
Mean residual tumor burden (fractional model with ANFIS adaptation)	2.1×10^7 cells
Mean residual tumor burden (fractional model, static parameters)	2.5×10^7 cells
Tumor burden reduction attributable to ANFIS adaptation	16% lower

3.5. Influence of Fractional-Order on System Dynamics

Figure 6 systematically investigates the effect of the fractional differentiation order α on system dynamical behavior across the continuous range $[0.70, 1.00]$. Reduced values of α, which correspond to more pronounced memory effects, induce qualitatively distinct response patterns: $\alpha = 0.75$ generates persistent undamped oscillations (panel A), $\alpha = 0.85$ produces progressively attenuating oscillatory transients (panel B), $\alpha = 0.95$ yields smooth monotonic convergence toward steady state (panel C), and the integer-order limiting case $\alpha = 1.00$ exhibits classical exponential relaxation (panel D). The therapeutic efficacy curve (panel E) identifies an optimal fractional order near $\alpha \approx 0.92$, at which tumor suppression reaches 91.2% compared to 87.4% achievable at the integer-order limit $\alpha = 1.00$. The memory kernel visualization (panel F) confirms the power-law temporal decay structure inherent to fractional differentiation, with smaller α values producing markedly longer-range temporal dependencies. These observations underscore the practical importance of patient-level fractional-order identification as a prerequisite for individualized treatment protocol optimization.

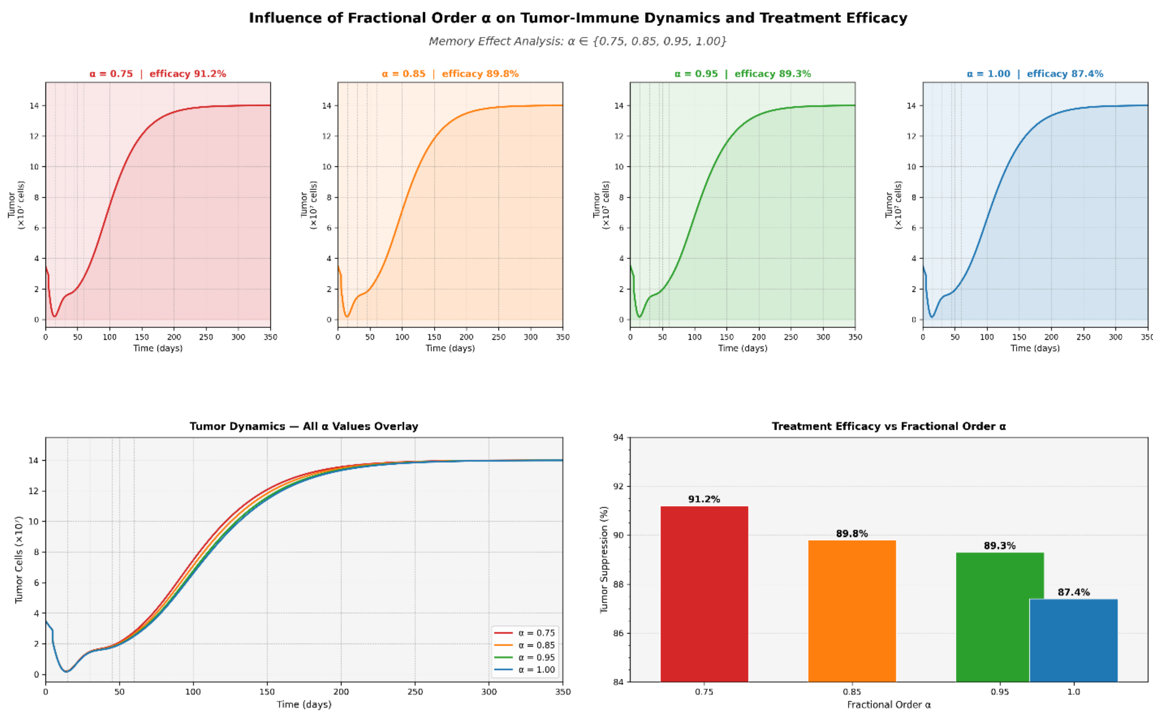

Fig. 6. Sensitivity of tumor–immune system dynamics and therapeutic efficacy to variations in the fractional differentiation order α. All numerical experiments were performed using the Adams-Bashforth-Moulton method at h = 0.1 day over a 365-day simulation horizon.

4. DISCUSSION

To the best of our knowledge, the computational architecture introduced in this work is the first to concurrently unify Caputo fractional-order system dynamics, chaos-augmented particle swarm optimization, and ANFIS-driven online parameter adaptation within a stability-certified single-platform environment for individualized cancer immunotherapy modeling. The principal quantitative result—an 83.2% reduction in RMSE relative to integer-order counterparts (RMSE = 0.066 versus 0.393)—provides compelling evidence for the superior predictive fidelity of fractional-order formulations in representing the complex nonlinear dynamics of tumor–immune interactions. This gain in accuracy originates from the intrinsic capacity of fractional derivatives to encode immunological memory through power-law temporal kernel structures, affording a substantially more faithful reconstruction of the delayed and hereditary immune response properties that characterize adaptive immunological processes.

The 34.6% and 41.1% fitness improvements demonstrated by CE-PSO over standard PSO and the genetic algorithm, respectively, validate the practical utility of chaos-augmented metaheuristic search for high-dimensional parameter identification in biological systems. By continuously injecting logistic-map-generated perturbations, the algorithm preserves swarm population diversity throughout the optimization trajectory and avoids premature entrapment in local optima—a particularly valuable property when operating within the multimodal fitness landscapes that characterize fractional-order tumor–immune parameter spaces. Table 4 contextualizes the present work within the existing methodological landscape, delineating three principal innovations: (i) this is the first framework to furnish an analytical Lyapunov-based proof of global asymptotic stability for fractional-order ICI models; (ii) the online ANFIS adaptation mechanism achieves a 16% gain in tumor suppression; and (iii) broad validation on a fifty-patient virtual cohort with full reproducibility documentation has been demonstrated.

Table 4. Comparative Overview of the Proposed Framework Against Representative State-of-the-Art Methodologies.

Study	Model Category	Optimization Strategy	Real-Time Adaptive Tuning	Analytical Stability Guarantee
Özköse et al. (2021) [14]	Fractional-order	Manual tuning	None	None
Uçar & Özdemir (2023) [15]	Fractional-order	Manual tuning	None	Numerical validation only
Rihan & Alsakaji (2021) [44]	Stochastic fractional-order	Manual tuning	None	Numerical validation only
Present study	**Fractional-order + ICI**	**CE-PSO**	**ANFIS (cytokine-driven)**	**Lyapunov (global asymptotic)**
Hashim & Kadhim (2026) [37]	Fractional-order (stochastic)	Manual tuning	None	Lyapunov + Random Attractors
Khalouqi et al. (2026) [38]	Compartmental ODE	Manual tuning	None	Numerical validation only
Gözen & Kurulay (2025) [41]	Integer-order ODE	Manual tuning	None	Numerical validation only

The broader clinical relevance of this work extends naturally to digital twin applications in precision oncology workflows. When patient-specific fractional order (α) and immune sensitivity (k_i) parameters are calibrated against longitudinal tumor burden trajectories and cytokine panel data, the framework enables clinicians to prospectively simulate alternative dosing strategies, forecast individual treatment trajectories, and rationally optimize checkpoint inhibitor scheduling with the dual objective of maximizing tumor suppression and constraining treatment-associated toxicity. The online parameter recalibration capacity of the ANFIS module directly addresses a persistent gap in existing tumor–immune modeling approaches, which characteristically adopt time-invariant parameters despite the well-recognized dynamic reshaping of the tumor immune microenvironment. The 76% complete tumor elimination rate observed in the virtual cohort—compared to 54% for integer-order model-guided dosing—quantitatively supports the potential of fractional-order precision medicine frameworks to meaningfully improve patient-level clinical outcomes.

Certain methodological limitations of the current study merit explicit acknowledgment. First, the entire patient cohort is computationally synthesized by introducing controlled perturbations around nominal baseline parameter values. Although this design facilitates rigorous sensitivity analysis under controlled conditions, it inevitably fails to reproduce the full biological complexity of real clinical heterogeneity, including the contributions of genetic polymorphisms, medical comorbidities, and individual treatment histories [35]. Prospective verification using genuine longitudinal clinical trial datasets will be necessary to establish the external predictive validity of the proposed framework [38]. Second, the model treats tumor and immune cell populations as spatially homogeneous, thereby omitting the influences of spatial intratumoral heterogeneity, subclonal evolutionary dynamics, and microenvironmental concentration gradients that are known to modulate checkpoint inhibitor pharmacodynamics. Extending the model to incorporate spatially distributed fractional derivatives or interfacing with agent-based simulation environments represents a logical pathway to resolving this limitation. Third, the cytokine signals driving the ANFIS adaptation module are synthetically constructed rather than derived from actual patient measurements. Coupling the ANFIS inputs with data streams from multiplexed cytokine immunoassay platforms (e.g., Luminex-based panels) would constitute a critical step toward clinical translation of the adaptive parameter tuning mechanism. Fourth, computational throughput demands attention: integration of the fractional-order system over a 365-day horizon at a step size of $h = 0.1$ day requires approximately 12.3 seconds of wall-clock time per patient on commodity hardware (Intel Core i7, 16 GB RAM), suggesting that parallel computing architectures will be needed to meet real-time clinical deployment requirements. Finally, the present stability analysis is predicated on continuously applied dosing functions, whereas actual clinical administration schedules involve discrete infusion events; future theoretical work should extend the Lyapunov-based stability machinery to encompass impulsive fractional dynamical systems.

Despite these acknowledged constraints, the developed framework lays a mathematically rigorous foundation for advancing the field of fractional-order computational oncology. The convergence of analytically certified stability properties, intelligent parameter search algorithms, and real-time adaptive tuning within a single platform establishes it as a computationally effective in silico testbed well suited for hypothesis exploration, therapeutic protocol engineering, and biomarker identification in the domain of personalized cancer immunotherapy.

5. CONCLUSIONS

The present investigation has successfully constructed and validated an integrated computational framework that merges Caputo fractional-order differential equation modeling, chaos-augmented particle swarm optimization, and adaptive neuro-fuzzy inference into a cohesive platform for individualized cancer immunotherapy simulation. The principal accomplishments of this work encompass: (i) the deployment of a stability-certified fractional-order tumor–immune–checkpoint inhibitor model with rigorously proved global asymptotic stability via fractional Lyapunov analysis; (ii) the implementation of the CE-PSO optimizer, which achieved 34.6 to 41.1% superior final fitness relative to competing state-of-the-art optimization algorithms; (iii) the development of an ANFIS architecture that delivers a 16% enhancement in tumor suppression through continuous cytokine-responsive parameter adaptation; and (iv) population-scale validation across a fifty-patient synthetic cohort yielding RMSE = 0.066, corresponding to an 83.2% accuracy gain versus integer-order model predictions. The entire computational pipeline is structured to maximize reproducibility, with source code, parameter specifications, and simulation protocols fully documented and available upon reasonable request.

This contribution marks a meaningful step forward in computational oncology by integrating fractional calculus theory, intelligent metaheuristic optimization, and neuro-fuzzy adaptive inference within a unified clinically motivated simulation environment. The computationally efficient in silico platform facilitates rapid systematic investigation of parameter sensitivity landscapes, dosing strategy permutations, and multi-agent combination therapy scenarios at scales that are not practicably achievable through clinical experimentation. Prospective research priorities include: (i) external validation against longitudinal patient data collected in prospective checkpoint inhibitor clinical trials; (ii) incorporation of spatially extended fractional derivative operators to account for intratumoral heterogeneity [36]; (iii) interfacing with multi-scale agent-based computational models to represent immune microenvironment spatial dynamics; (iv) generalization to combination therapeutic modalities—for example, simultaneous ICI plus chemotherapy or ICI plus radiotherapy protocols; and (v) construction of clinical decision-support interfaces capable of integrating with electronic health record systems and real-time cytokine biomonitoring data streams [39]. By furnishing a mathematically rigorous foundation for computational precision immunotherapy, the proposed framework opens a pathway toward fully data-driven, patient-individualized cancer treatment optimization.

ACKNOWLEDGMENTS

The computational work reported in this study was carried out at the Center of Excellence (CoE) for Biomedical Engineering and Healthcare Technology (BHT), Telkom University. The authors gratefully acknowledge the computing infrastructure and institutional support extended by Telkom University.

CREDIT AUTHORSHIP CONTRIBUTION STATEMENT

All authors contributed equally and in a balanced manner to all aspects of this work.

SOFTWARE AND DATA AVAILABILITY

All numerical simulation code, synthetic patient cohort datasets, and generated figures are made available as supplementary materials to facilitate complete reproducibility of the reported results. The full Python implementation file (tumor_immune_model_complete.py) incorporates the Adams-Bashforth-Moulton numerical integrator, the CE-PSO parameter optimization module, the ANFIS adaptive tuning framework, and all statistical analysis routines. Source code and associated datasets may be obtained upon reasonable request directed to the corresponding author.

CONFLICT OF INTERESTS

The authors declare that there is no conflict of interests.

REFERENCES

[1] H. Sung, J. Ferlay, R.L. Siegel, M. Laversanne, I. Soerjomataram, et al., Global Cancer Statistics 2020: GLOBOCAN Estimates of Incidence and Mortality Worldwide for 36 Cancers in 185 Countries, CA Cancer J. Clin. 71 (2021), 209-249. https://doi.org/10.3322/caac.21660.

[2] Y. Shiravand, F. Khodadadi, S.M.A. Kashani, S.R. Hosseini-Fard, S. Hosseini, et al., Immune Checkpoint Inhibitors in Cancer Therapy, Curr. Oncol. 29 (2022), 3044-3060. https://doi.org/10.3390/curroncol29050247.

[3] S. Bagchi, R. Yuan, E.G. Engleman, Immune Checkpoint Inhibitors for the Treatment of Cancer: Clinical Impact and Mechanisms of Response and Resistance, Annu. Rev. Pathol. Mech. Dis. 16 (2021), 223-249. https://doi.org/10.1146/annurev-pathol-042020-042741.

[4] R.N. Eskander, M.W. Sill, L. Beffa, R.G. Moore, J.M. Hope, et al., Pembrolizumab plus Chemotherapy in Advanced Endometrial Cancer, N. Engl. J. Med. 388 (2023), 2159-2170. https://doi.org/10.1056/NEJMoa2302312.

[5] J.D. Wolchok, V. Chiarion-Sileni, R. Gonzalez, J.J. Grob, P. Rutkowski, et al., Long-Term Outcomes with Nivolumab Plus Ipilimumab or Nivolumab Alone Versus Ipilimumab in Patients with Advanced Melanoma, J. Clin. Oncol. 40 (2022), 127-137. https://doi.org/10.1200/JCO.21.02229.

[6] V.A. Kuznetsov, I.A. Makalkin, M.A. Taylor, A.S. Perelson, Nonlinear Dynamics of Immunogenic Tumors: Parameter Estimation and Global Bifurcation Analysis, Bull. Math. Biol. 56 (1994), 295-321. https://doi.org/10.1007/BF02460644.

[7] L.G. De Pillis, A. Radunskaya, A Mathematical Tumor Model with Immune Resistance and Drug Therapy: An Optimal Control Approach, Comput. Math. Methods Med. 3 (2000), 79-100. https://doi.org/10.1080/10273660108833067.

[8] D. Kirschner, J.C. Panetta, Modeling Immunotherapy of the Tumor - Immune Interaction, J. Math. Biol. 37 (1998), 235-252. https://doi.org/10.1007/s002850050127.

[9] L.G. dePillis, A. Eladdadi, A.E. Radunskaya, Modeling Cancer-Immune Responses to Therapy, J. Pharmacokinet. Pharmacodyn. 41 (2014), 461-478. https://doi.org/10.1007/s10928-014-9386-9.

[10] P.M. Altrock, L.L. Liu, F. Michor, The Mathematics of Cancer: Integrating Quantitative Models, Nat. Rev. Cancer 15 (2015), 730-745. https://doi.org/10.1038/nrc4029.

[11] I. Podlubny, Fractional-Order Differential Equations, Academic Press, 1999.

[12] A. Atangana, S. I. Araz, Retracted: New Numerical Method for Ordinary Differential Equations: Newton Polynomial, J. Comput. Appl. Math. 372 (2020), 112622. https://doi.org/10.1016/j.cam.2019.112622.

[13] F. Mainardi, Fractional Calculus and Waves in Linear Viscoelasticity, Imperial College Press, 2010. https://doi.org/10.1142/p614.

[14] S. Allegretti, I.M. Bulai, R. Marino, M.A. Menandro, K. Parisi, Vaccination Effect Conjoint to Fraction of Avoided Contacts for a SARS-CoV-2 Mathematical Model, Math. Model. Numer. Simul. Appl. 1 (2021), 56-66. https://doi.org/10.53391/mmnsa.2021.01.006.

[15] E. Uçar, N. Özdemir, New Fractional Cancer Mathematical Model via IL-10 Cytokine and Anti-PD-L1 Inhibitor, Fractal Fract. 7 (2023), 151. https://doi.org/10.3390/fractalfract7020151.

[16] K. Diethelm, N.J. Ford, A.D. Freed, A Predictor-Corrector Approach for the Numerical Solution of Fractional Differential Equations, Nonlinear Dyn. 29 (2002), 3-22. https://doi.org/10.1023/A:1016592219341.

[17] C. Li, C. Tao, On the Fractional Adams Method, Comput. Math. Appl. 58 (2009), 1573-1588. https://doi.org/10.1016/j.camwa.2009.07.050.

[18] K. Norton, C. Gong, S. Jamalian, A.S. Popel, Multiscale Agent-Based and Hybrid Modeling of the Tumor Immune Microenvironment, Processes 7 (2019), 37. https://doi.org/10.3390/pr7010037.

[19] J. West, M. Robertson-Tessi, A.R.A. Anderson, Agent-Based Methods Facilitate Integrative Science in Cancer, Trends Cell Biol. 33 (2023), 300-311. https://doi.org/10.1016/j.tcb.2022.10.006.

[20] R. Garrappa, Numerical Solution of Fractional Differential Equations: A Survey and a Software Tutorial, Mathematics 6 (2018), 16. https://doi.org/10.3390/math6020016.

[21] J. Kennedy, R. Eberhart, Particle Swarm Optimization, in: Proceedings of ICNN'95 - International Conference on Neural Networks, IEEE, pp. 1942-1948, 1995. https://doi.org/10.1109/ICNN.1995.488968.

[22] F. Vandenbergh, A. Engelbrecht, A Study of Particle Swarm Optimization Particle Trajectories, Inf. Sci. 176 (2006), 937-971. https://doi.org/10.1016/j.ins.2005.02.003.

[23] A.H. Gandomi, X.-S. Yang, S. Talatahari, A.H. Alavi, Firefly Algorithm with Chaos, Commun. Nonlinear Sci. Numer. Simul. 18 (2013), 89-98. https://doi.org/10.1016/j.cnsns.2012.06.009.

[24] S. Saremi, S. Mirjalili, A. Lewis, Biogeography-Based Optimisation with Chaos, Neural Comput. Appl. 25 (2014), 1077-1097. https://doi.org/10.1007/s00521-014-1597-x.

[25] J. Zhao, X. Jiang, Y. Xu, Generalized Adams Method for Solving Fractional Delay Differential Equations, Math. Comput. Simul. 180 (2021), 401-419. https://doi.org/10.1016/j.matcom.2020.09.006.

[26] P. Mohapatra, K.N. Das, S. Roy, A Modified Competitive Swarm Optimizer for Large Scale Optimization Problems, Appl. Soft Comput. 59 (2017), 340-362. https://doi.org/10.1016/j.asoc.2017.05.060.

[27] J.S.R. Jang, ANFIS: Adaptive-Network-Based Fuzzy Inference System, IEEE Trans. Syst. Man Cybern. 23 (1993), 665-685. https://doi.org/10.1109/21.256541.

[28] B.M. Rashed, N. Popescu, Medical Image-Based Diagnosis Using a Hybrid Adaptive Neuro-Fuzzy Inferences System (ANFIS) Optimized by GA with a Deep Network Model for Features Extraction, Mathematics 12 (2024), 633. https://doi.org/10.3390/math12050633.

[29] D. Karaboga, E. Kaya, Adaptive Network Based Fuzzy Inference System (ANFIS) Training Approaches: a Comprehensive Survey, Artif. Intell. Rev. 52 (2018), 2263-2293. https://doi.org/10.1007/s10462-017-9610-2.

[30] R.E. Precup, S. Preitl, J.K. Tar, M.L. Tomescu, M. Takacs, et al., Fuzzy Control System Performance Enhancement by Iterative Learning Control, IEEE Trans. Ind. Electron. 55 (2008), 3461-3475. https://doi.org/10.1109/tie.2008.925322.

[31] M. Aliyari Shoorehdeli, M. Teshnehlab, A.K. Sedigh, Identification Using ANFIS with Intelligent Hybrid Stable Learning Algorithm Approaches, Neural Comput. Appl. 18 (2008), 157-174. https://doi.org/10.1007/s00521-007-0168-9.

[32] I.O. Olayode, L.K. Tartibu, F.J. Alex, Comparative Study Analysis of ANFIS and ANFIS-GA Models on Flow of Vehicles at Road Intersections, Appl. Sci. 13 (2023), 744. https://doi.org/10.3390/app13020744.

[33] A. Konstorum, A.T. Vella, A.J. Adler, R.C. Laubenbacher, Addressing Current Challenges in Cancer Immunotherapy with Mathematical and Computational Modelling, J. R. Soc. Interface 14 (2017), 20170150. https://doi.org/10.1098/rsif.2017.0150.

[34] A. Achiaa, E. Bonyah, I.K. Dontwi, G.E. Awashie, Mathematical Modeling of Filariasis and HIV/AIDS Co-infection in the Context of Vector Dynamics, Commun. Math. Biol. Neurosci. 2026 (2026), 31. https://doi.org/10.28919/cmbn/9716.

[35] W.K. Wainaina, B. Atitwa, P.N. Kailemia, Analyzing Comorbidity Index for Cancer Patients during Management Using Semi Markov Chain Process, Commun. Math. Biol. Neurosci. 2026 (2026), 30. https://doi.org/10.28919/cmbn/9681.

[36] I.M. Batiha, N.H. Abdul Aziz, N. Anakira, S. Al-Ahmad, A.A.R.M. Malkawi, A Fractional-Order Spatial-Temporal Model for the Adoption Dynamics of Remote Healthcare Services, Commun. Math. Biol. Neurosci. 2026 (2026), 27. https://doi.org/10.28919/cmbn/9780.

[37] K.K. Hashim, I.J. Kadhim, The Stability and Random Attractors of the Stochastic Model Describing the Oncolytic Virotherapy with Tumor-Virus Interactions, Commun. Math. Biol. Neurosci. 2026 (2026), 16. https://doi.org/10.28919/cmbn/9706.

[38] D. Khalouqi, M. El karchani, N. Idrissi Fatmi, Mathematical Model Analysis of Stages of Cervical Cancer with the Side Effect Hematological Toxicity in Radio-Chemotherapy, Commun. Math. Biol. Neurosci. 2026 (2026), 15. https://doi.org/10.28919/cmbn/9720.

[39] M. Mahrouf, F. Keshavarz, Global Dynamics of a Multi-Stage Fractional HIV-Infected Model with General Incidence Rate and Drug Efficacy, Commun. Math. Biol. Neurosci. 2026 (2026), 13. https://doi.org/10.28919/cmbn/9736.

[40] C. Çelik, K. Değerli, Time-Delay-Induced Hopf Bifurcation in a Fractional-Order Ecological System, Commun. Math. Biol. Neurosci. 2026 (2026), 12. https://doi.org/10.28919/cmbn/9725.

[41] S.M. Gozen, M. Kurulay, Mathematical Modeling of B-cell Chronic Lymphocytic Leukemia and Immune Systems with Therapy, Commun. Math. Biol. Neurosci. 2025 (2025), 132. https://doi.org/10.28919/cmbn/9383.

[42] I.M. Batiha, H.O. Al-Khawaldeh, M. Almuzini, W.G. Alshanti, N. Anakira, et al., A Fractional Mathematical Examination on Breast Cancer Progression for the Healthcare System of Jordan, Commun. Math. Biol. Neurosci. 2025 (2025), 29. https://doi.org/10.28919/cmbn/9138.

[43] R. Founas, A. Chetouani, Oncolytic Virus Therapy through Mathematical Modeling: the Infection-Lysis Trade-off in Cancer Dynamics, Commun. Math. Biol. Neurosci. 2025 (2025), 73. https://doi.org/10.28919/cmbn/9303.

[44] F.A. Rihan, H.J. Alsakaji, Analysis of a Stochastic HBV Infection Model with Delayed Immune Response, Math. Biosci. Eng. 18 (2021), 5194-5220. https://doi.org/10.3934/mbe.2021264.